Intermetallics 121 (2020) 106780

Contents lists available at ScienceDirect

Intermetallics

journal homepage: http://www.elsevier.com/locate/intermet

Sub-grain formation in Al–Li–Mg–Zn–Cu lightweight entropic alloy by ultrasonic hammering

Ruixuan Li [a], Xin Li [b], Jiang Ma [b], Yong Zhang [a,**]

[a] Beijing Advanced Innovation Center of Materials Genome Engineering, State Key Laboratory for Advanced Metals and Materials, University of Science and Technology Beijing, Beijing, 100083, China
[b] College of Mechatronic and Control Engineering, Shenzhen University, Shenzhen, 518060, China

ARTICLE INFO

Keywords:
Ultrasonic hammering
Entropic alloys
Grain size
Sub-grain formation
Hardness improvement
Modulus improvement

ABSTRACT

In this paper, the ultrasonic hammering treatment is applied to the lightweight entropic alloy $Al_{80}Li_5Mg_5Zn_5Cu_5$, contributing to the modification of coarse microstructures and the improvement of mechanical properties. The effects of ultrasonic hammering on the microstructures and mechanical properties of $Al_{80}Li_5Mg_5Zn_5Cu_5$ are elaborately studied, and the formation of sub-grains is thoroughly analyzed. Results show that the coarse dendrite structure is crushed into diffusely distributed micron-sized particles, and the grain size is refined significantly from larger than 200 μm to about5 μm, along with the formation of sub-grains during instant dynamic recovery. Microhardness and modulus of the grain-refined alloy increase by 50% and 22%, respectively, compared to the coarse-grained counterpart without ultrasonic hammering.

1. Introduction

Property enhancement through grain refinement to micro/nano-scale has been extensively investigated in various alloys over the past years, both in bulk alloys [1,2] and surface layers of bulk materials [3]. Compared with grain refinement in bulk alloys, preparing well-bonded and hard layers with compressive residual stresses and small-sized grains provides more promising practical industrial applicability. Surface modification is proved to be effective to enhance the corrosion resistance, fatigue strength, wear resistance, and more importantly, reduce the cost [4–6]. Among various methods, high-intensity ultrasonic vibration, as a useful power source characterized by lower energy input and shorter treatment time, has aroused wide public concern for homogenizing microstructure, refining grains, and optimizing the overall performance, whether in liquid [7–9] or solid alloys. In terms of the solid-state metals, ultrasonic surface treatment has been developed using different names, such as surface mechanical attrition treatment (SMAT) [10,11], ultrasonic impact peening (UIP) [12,13], surface mechanical grinding treatment (SMGT) [3,14], ultrasonic surface rolling process (USRP) [15], and nanocrystal surface modification (NSM) [16,17].

Among all the ultrasonic-related treatments, the ultrasonic hammering (UH) technique is the newly developed one, and has been proved to be useful in thermoplastic forming of bulk metallic glasses. J. Ma et al. successfully fabricated a series of metallic glasses from micro-length scale to macro-length scale, by employing ultrasonic vibration and molten plastics viscous medium [18–20]. Later, through establishing atomic bondings between ribbons at a low temperature, they demonstrated an effective ultrasound-enabled joining approach to synthesize metallic glass-glass composites [21].

Having similar historical origins as amorphous alloys, high entropy alloys have attracted much public attention for their outstanding comprehensive properties [22–26]. By combing the low density of Aluminum (Al) alloys and high strength and ductility of high entropy alloys, the lightweight entropic alloy $Al_{80}Li_5Mg_5Zn_5Cu_5$ has been studied in our previous research works [27,28], and has been chosen in this work. It is reported to have a similar density to traditional Al alloys, while exhibiting much higher strength and hardness. Moreover, this alloy is also predicted to show high corrosion resistance and high thermo-stability due to the high entropy effect. In this paper, the high intensity and high frequency UH is applied to the entropic alloy $Al_{80}Li_5Mg_5Zn_5Cu_5$. Changes in microstructures, grain sizes, and hardness, and the related reasons have been comprehensively analyzed.

* Corresponding author.
E-mail address: drzhangy@ustb.edu.cn (Y. Zhang).

https://doi.org/10.1016/j.intermet.2020.106780
Received 31 December 2019; Received in revised form 17 March 2020; Accepted 17 March 2020
0966-9795/© 2020 Elsevier Ltd. All rights reserved.

2. Experiments

The raw materials used in the experiments were pure aluminum [99.9 wt.% (weight percent) purity] ingots, pure zinc (99.9 wt.% purity) ingots, magnesium-lithium alloys (Mg-20 wt.%Li) and pure copper (99.9 wt.% purity) ingots. Al–Li–Mg–Zn–Cu alloy ingots with a nominal chemical composition of $Al_{80}Li_5Mg_5Zn_5Cu_5$ [in at.% (atomic percent)] were melted in a vacuum induction melting (VIM) furnace under Argon atmosphere, and cut into small cylinders with the size of Φ3mm*2 mm. Then, high-frequency hammering is applied on the surface.

The apparatus (schematically shown in Fig. 1(a)) in this work is made up of a transducer (converting electrical energy to vibrations), a booster (amplifying the amplitude of vibrations), and a horn (transferring mechanical vibrations to the sample). Compared to other ultrasonic-related surface treatments, it is very different in the mechanism. In this UH experiment, the horn is brought into contact with the sample under the trigger force ***F***, and then it begins to vibrate at a predefined amplitude. The vibration time can last from several milliseconds to several seconds according to the processing parameters, and the actual interacting time towards the sample is determined by the trigger force. As shown in Fig. 1(b), when $\boldsymbol{F} = 0$, the horn is in contact with the sample within half a period of ultrasonic vibration, and with higher values of ***F***, the fraction of time in which the horn is in direct contact with the sample increases. Until finally, the horn always remains in contact with the sample and there is no hammering effect.

In this experiment, the 2020 ultrasonic plastic welding machine produced by Shenzhen Hongri Ultrasonic Equipment Co., Ltd. (Shenzhen, China) was used. The ultrasonic amplitude and frequency used in the experiment were 50 μm and 20 kHz, respectively. The ultrasonic energy, the applied pressure, and the holding time were set as 150 J, 0.15 MPa, and 0.01 s, respectively.

Determination of microstructures was carried out on a field-emission scanning electron microscopy (SEM, Auriga Field Emission Scanning Electron Microscope, Carl Zeiss, Germany) equipped with an energy dispersive X-ray spectrometer (EDX) and an electron backscattered diffraction (EBSD). The phase structures were analyzed by an X-ray diffractometer (XRD, BRUKERD8 Discover, Germany) using Cu Kα radiation. To characterize the hardness and Young's modulus of the $Al_{80}Li_5Mg_5Zn_5Cu_5$ alloys before and after UH treatment, nano-indentation experiments were conducted using a Berkovich triangular pyramid indenter with a tip radius of 20 nm. The Poisson's ratio and elastic modulus of the indenter tip were 0.07 and 1.141 × 106 MPa, respectively. To ensure the accuracy of the tested point, the valid indentation depth was maintained at 10% thickness of the ultrasonic-treated layer.

3. Results

3.1. Microstructures

Fig. 2(a) and (b) show the microstructures of as-cast samples before UH processing at low and high magnification, respectively. The actual compositions of the alloy and phases detected by EDX are shown in Table 1. Note that the element Li is difficult to be detected by EDX and is ignored in the following experiments, because the use of master alloy Mg-20 wt%Li fixes the atomic percentage of Li and Mg, and because the mass percentage of Li is very small in the alloy. In addition, the effect of Li is not our focus. There is a little difference between the nominal and actual alloy composition, because some elemental vaporization may occur during vacuum melting. Combined with EDX analysis, three kinds of phases can be observed, including Al, Al_2Cu, and Al–Zn–Mg–Cu phase. In Fig. 2(a), a dendritic structure is exhibited in the as-cast alloy, where the FCC-Al matrix has a black contrast, the intermetallic phases Al_2Cu have a grey contrast, and the Al–Zn–Mg–Cu phase has a bright contrast.

Fig. 2(c) and (d) exhibit the upper surface of the sample after UH treatment at low and high magnification, respectively, and Fig. 2(e) is the SEM image from the cross-sectional area. It is evident that there is a significant microstructural alteration, and the thickness of this deformation layer is about 3–5 μm. The coarse dendrites are crushed into small particles and diffusely distributed in the Al phase, and the size distribution of the intermetallics before and after hammering are plotted in Fig. 2(f), through measuring more than 100 crushed particles. As the original dendrites are very coarse and they connect into a large network, their sizes are considered greater than 10 μm. In terms of the crushed intermetallics, the average size is counted as ~2 μm, and their volume

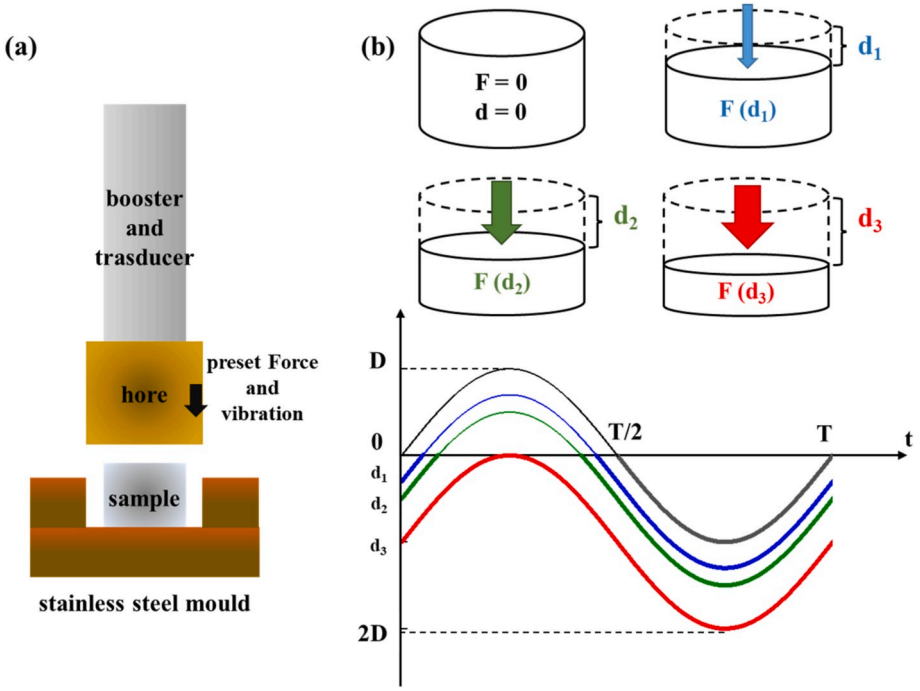

Fig. 1. (a) The ultrasonic hammering apparatus; (b) Relationship between trigger force and contact time (thick lines) when the ultrasonic is applied.

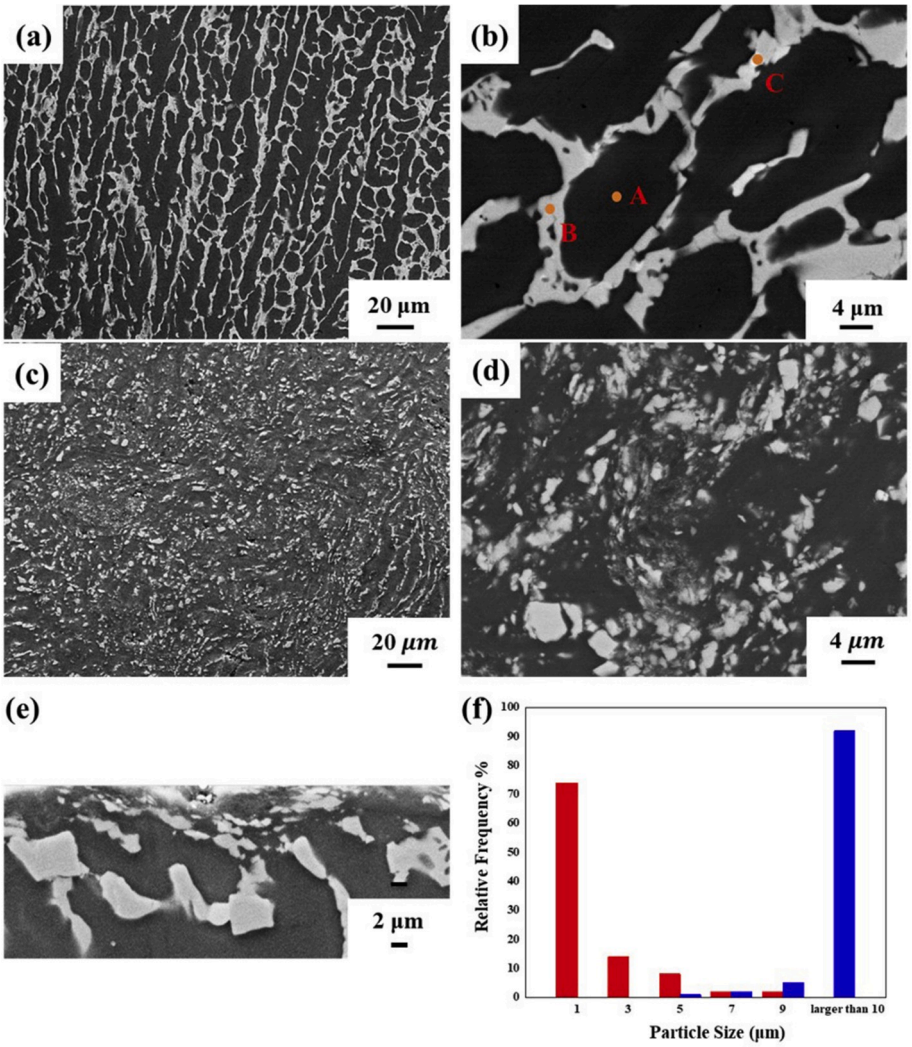

Fig. 2. (a) Low magnification and (b) high magnification of $Al_{80}Li_5Mg_5Zn_5Cu_5$ alloys before UH treatment. (c) Low magnification and (d) high magnification of upper surface layer after UH treatment. (e) The cross-sectional area after UH treatment. (f) Particle size-frequency distribution of the original (blue column) and crushed (red column) intermetallics. (For interpretation of the references to color in this figure legend, the reader is referred to the Web version of this article.)

Table 1
Detailed compositions of alloys and different phases. Note that the element Li is difficult to be detected by EDX and is ignored in the following experiments, because the use of master alloy Mg-20 wt%Li fixes the atomic percentage of Li and Mg, and the mass percentage of Li is very small in the alloy. In addition, the effect of Li is not our focus.

Composition (at %)	Al	Mg	Zn	Cu
Sample	85.61	4.66	4.89	4.83
A	94.12	1.55	2.84	1.49
B	64.65	7.81	4.84	22.70
C	26.37	19.79	42.53	11.31

fraction is estimated as ~26%, when assuming that all of the crushed particles are spherical and that the volume fraction is approximately equal to the area fraction.

Fig. 3 shows the XRD patterns of the $Al_{80}Li_5Mg_5Zn_5Cu_5$ sample before and after ultrasonic modification, and it shows that there is obviously no phase transformation when the UH treatment is applied. The α-Al and Al_2Cu phases are revealed by the diffraction peaks, which is consistent with the SEM and EDS results. There are also some small peaks from the $MgZn_2$ phase, and they actually correspond to the phase with the composition of Mg $(Zn, Cu)_2$, because of the elemental similarity and replacement. The intensity of the diffraction peaks of α-Al

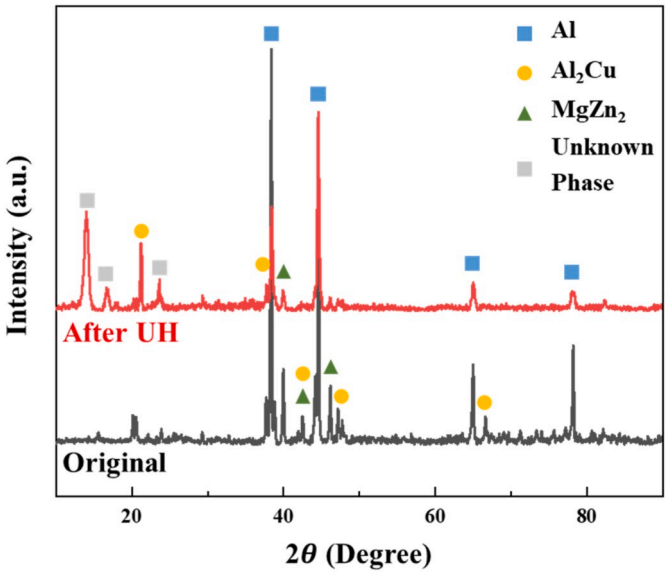

Fig. 3. XRD profile of the alloy before and after UH treatment.

phase exceeds that of the other phases, also suggesting a predominant volume fraction of the α-Al phase. The unknown phases after hammering may come from two aspects: the ternary or even quaternary phases may appear under the high-entropy effect and the complex interaction; the diffraction peaks of the plasticine substrate is detected during the experiment because the sample size is too small.

3.2. Grain sizes

The changes of grain size before and after ultrasonic treatment are depicted by Fig. 4, which illustrates that coarse equiaxed grains on the surface suddenly evolve into fine equiaxed sub-grains, without obvious flattening or elongating. The original grain size is ~200 μm as shown in Fig. 4(a1) and (c1). Fig. 4(b1) shows the phase map from EBSD patterns, where the yellow, red, and black regions correspond to the Al phase, Al_2Cu phase, and blind zones, respectively. The typical dendritic structure can be identified only when black and red regions are added together. This can be attributed to the high-entropy composition and a large number of solute atoms in the Al_2Cu and Mg $(Zn, Cu)_2$ phase, which in turn cause severe lattice distortion and a large number of blind zones.

When the 20 kHz-UH is applied, although the Al phase does not seem to be much affected in the SEM pictures (Fig. 2), it is actually severely deformed and broken. Compared with the original sample in Fig. 4(b1), the increased blind zones (black areas) in Fig. 4(b2) result from the strong plastic deformation and high-density dislocation in the Al phase. Sub-grains with low-angle boundaries and the size of ~5 μm are formed in a single coarse grain, as shown in Fig. 4(a2) and (c2), and the reasons for them will be further analyzed in the Discussion section.

3.3. Hardness and modulus

Nano-indentation techniques are most frequently used to characterize the typical mechanical properties including the micro-hardness and Young's modulus. When the indenter is pressed into the specimen, elastic deformation occurs, followed by plastic deformation, which leads to the formation of a hardness impression conforming to the shape of the indenter. When the applied load is removed, only the elastic portion of the displacement is recovered, which facilitates the use of an elastic solution in modeling the contact process. A typical load-displacement curve as a function of tip penetration depth for the untreated and UH-treated specimens are shown in Fig. 5(a). It is evident that both two specimens have a maximum penetration depth of about 500 nm, while the maximum load increase from 8.7 to 12.5 mN after the effect of high-frequency hammering. Furthermore, these two similar load-displacement curves indicate a similar indentation-induced deformation mechanism during testing, that is to say, there is no occurrence of fracture events in both specimens as observed in Fig. 5(a).

UH treatment noticeably enhances the surface micro-hardness and modules of $Al_{80}Li_5Mg_5Zn_5Cu_5$ alloy, as shown in Fig. 5(b), which is averaged from six nano-indentation measurements. The micro-hardness of the original sample is only 1.5 GPa. After high-frequency hammering, it is increased by 50% and reaches about 2.25 GPa. In terms of the modulus, the introduction of 500 Hz-UH improves the elastic modulus considerably from 68 GPa to 78 GPa. The increase in mechanical behaviors of the UH-treated specimen compared to those of the untreated specimens may be attributed to the dispersion strengthening, dislocation strengthening, and grain boundary strengthening effect, and this will be further discussed in Section 4.

4. Discussion

4.1. Sub-grain formation

The concept of sub-grains was originally established in the field of creep, where plastic deformation can be carried out in high temperature

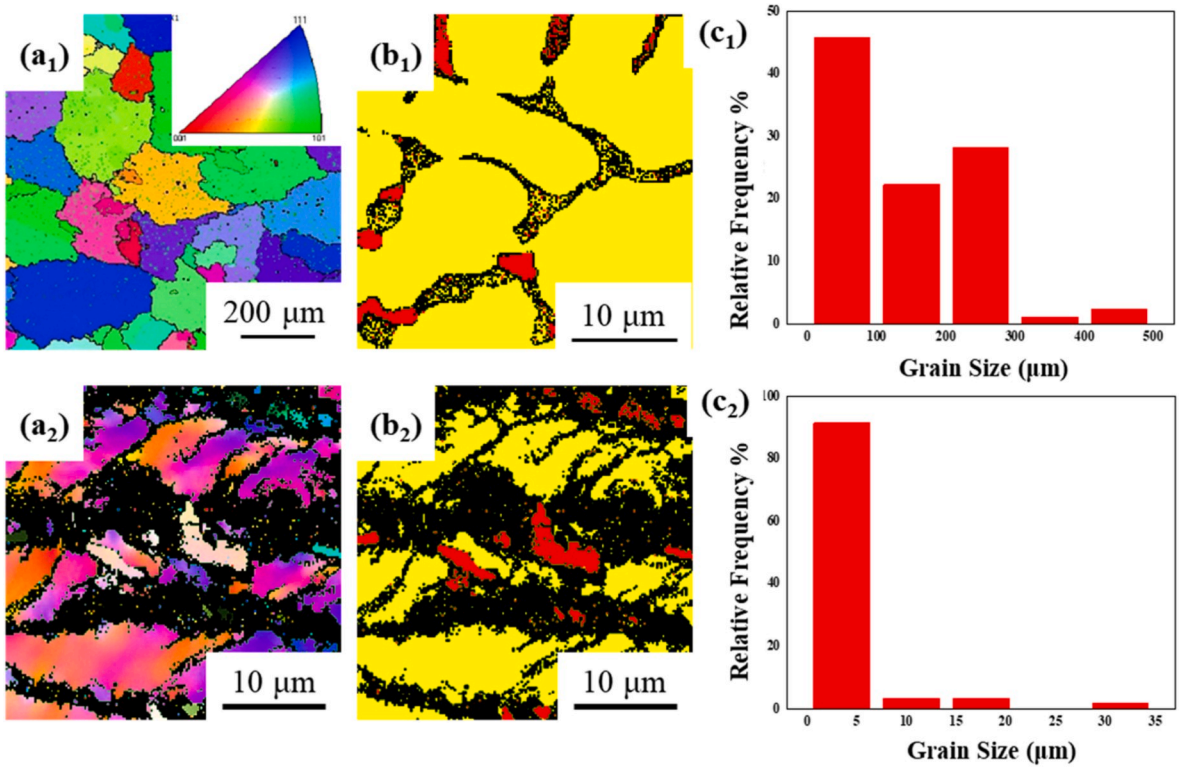

Fig. 4. (a_1) (a_2) EBSD images, (b_1) (b_2) phase map, and (c_1) (c_2) grain size distribution of the alloy before and after UH treatment, respectively. In (b_1) and (b_2), the yellow region refers to the Al-rich phase and the red region corresponds to the Al_2Cu phase. (For interpretation of the references to color in this figure legend, the reader is referred to the Web version of this article.)

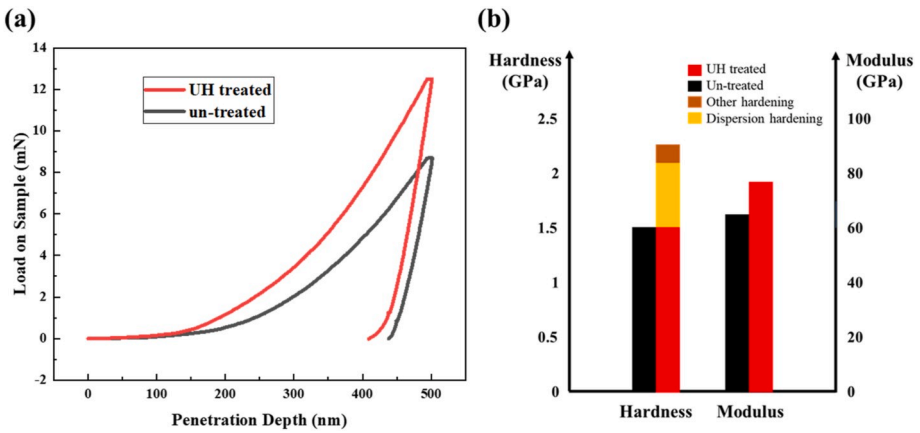

Fig. 5. (a) Load–displacement curve for the untreated and UH-treated specimens; (b) Comparison of the hardness and modulus between the original and UH-treated sample.

under a force lower than the yield stress. For Al-based alloys, due to the high stack fault energy and the narrow extended dislocation width, the dislocations tend to cancel each other out through cross slip and climbing. Therefore, dynamic recovery and sub-grain formation are more likely to be generated under the reduced local energy, instead of dynamic recrystallization. The sub-grain boundaries come close to ideal small-angle dislocation boundaries.

In our UH experiment, the energy of hammering is not only used to increase the internal temperature, but is also stored in high-density dislocations caused by the severe deformation, and it is also used to crush the continuous coarse dendrites, which is different from the hammering-treated amorphous alloys [18,19]. As shown in Fig. 6(a), with the sudden increase of local dislocation density, in order to keep work hardening at the lowest energy level, the number of active slip systems in a single crystal tends to locally decrease, compared with the number required by Taylor criterion for compatible deformation. In this case, crystals rotate and their orientations are changed because of the local preference of one slip system, which is driven by applied stress (Schmid factor). Similarly, from an energy perspective, the minimization of energy causes the long-range internal stresses caused by the deformation of the unit volume element to be partially offset by the deformation and the rotation of the adjacent unit volume element. Therefore, the number of active slip systems in each crystal changes, thus leading to geometrical softening or hardening. The inhomogeneous dislocations then act as the beginning of sub-grain boundaries, forced by the laws of non-linear continuum mechanics. These sub-grain formation has been explained by R. Sedlácek et al. [29–32] for the reason of the intrinsically developed inhomogeneity of plastic deformation.

The schematic of dislocation motion in a single crystal is shown in Fig. 6(b). Driven by the hammering energy, dislocations start to move, reorganize, polygonize, and tangle into dislocation cells. Then, the cell walls become thinner, sharper, and gradually change to sub-grains. Furthermore, the causes of non-recrystallized grains can also be attributed to the following two points: the pinning effect on dislocations from fine intermetallic particles, and the rapid suspension of the ultrasonic process. Therefore, energy is not high enough to affect the migration of

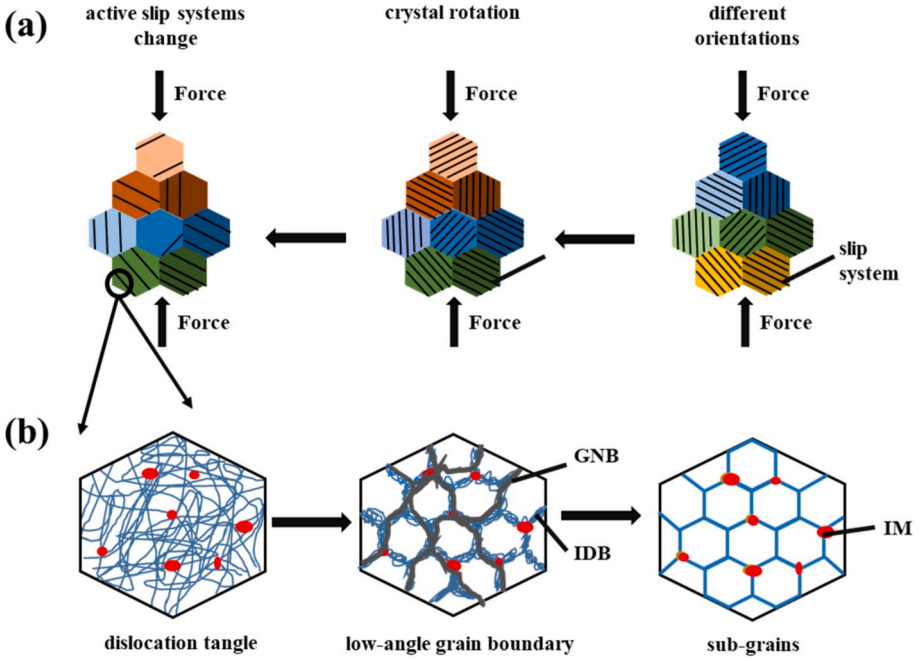

Fig. 6. (a) Origin of varying dislocation density and sub-grain formation during deformation, where the change of color means the change of crystal orientation; (b) Schematic of the dislocation motion in a single crystal, where GNB, IDB, and IM refer to the geometrically necessary dislocation, incidental dislocation boundary, and intermetallics, respectively. (For interpretation of the references to color in this figure legend, the reader is referred to the Web version of this article.)

large-angle grain boundaries. In our future experiments, the ultrasonic energy and time will be further increased, so that fine recrystallized grains and more optimized performance may be obtained.

4.2. Hardness and modulus improvement

After dendrites are crushed into small particles by the hammering effect, the elastic modulus is improved according to the nano-indentation results. Considering the alloy with dispersed intermetallic particles as a particle-reinforced composite, the mixing law of composites can be employed to analyze the elastic modulus changing, which is calculated as:

$$\frac{E_p E_m}{E_p V_m + E_m V_p} \leq E \leq E_m V_m + E_p V_p \quad (1)$$

where E_m is the modulus of original alloys tested as 64 GPa, and E_p is that of Al_2Cu (120 GPa) [33]. Here V_m (~74%) and V_p (~26%) are the volume fraction of matrix and intermetallics, respectively, and they are estimated from the SEM images in Fig. 2. It can be found that the elastic modulus after hammering (78 GPa) falls exactly between the upper (78.56 GPa) and lower limits (72.8 GPa). Therefore, the modulus of the surface layer after ultrasonic treatment can be successfully predicted by the mixing law.

As for the hardness improvement, there are several contributions. The sub-grain boundaries lead to hardening as they induce long-range internal back stresses in the interior of the sub-grains [29], and the diffusely distributed intermetallics cause strengthening by hindering dislocation motion. Here solid solution strengthening can be ignored because there is no change of solubility in the Al matrix before and after hammering. However, since the formation of sub-grains has a complex effect on the dislocation density, and the pinning effect of sub-grain boundaries is difficult to quantify, only strengthening effect from dispersed particles is analyzed here. Assuming that only Orowan bypass mechanism is activated, when dislocations pass through the hard and brittle intermetallics with an average diameter of 2 μm, hardness improvement from dispersion strengthening is estimated as [2,34–36]:

$$\Delta HV_p = CM \frac{0.81Gb}{2\pi\sqrt{1-\nu}} \ln\left(\frac{d}{b}\right)\left(0.615d\sqrt{\frac{2\pi}{3f}} - d\right)^{-1} \quad (2)$$

where C is the scaling factor between Vickers hardness and yield strength equal to 3.16; M is the mean orientation factor and M is equal to 3.06 for the face-centered cubic (FCC) polycrystalline matrix; G is the shear modulus, equal to 27 GPa for Al alloys; b is the magnitude of the Burgers vector (0.286 nm for Al); ν is the Poisson's ratio (0.3 for Al), d is the diameter of the crushed intermetallics, and f is the volume fraction of them. The average diameter and volume fraction have been estimated as 2 μm and 26%, respectively. Consequently, the calculated hardness improvement from dispersion hardening is about 57 HV.

The nano hardness value (GPa) can be converted into the Vickers hardness (HV/kg·mm^{-2}) using the conversion factor 92.65 [37], so the Vickers hardness improvement of the alloy after the hammering is estimated as 69.5 HV. It is evident that the dispersion strengthening accounts for about 80% of the total hardness improvement, implying that the UH treatment is an effective way to enhance micro-hardness mainly through crushing the dendrites. On the other hand, it is also indicated that the dislocation density is reduced after sub-grain formation, and the pinning effect of sub-grain boundaries on dislocations is obviously weaker than that of large-angle grain boundaries. It needs to be emphasized that the model we use here is really rough and we only aim to indicate the hardness contribution trend in the surface micro-hardness.

5. Conclusions

When the high-frequency ultrasonic hammering is applied on the $Al_{80}Li_5Mg_5Zn_5Cu_5$ lightweight entropic alloy, temperature rise, severe deformation, and dynamic recovery almost simultaneously occur in a short time span, which contributes to homogeneous microstructures, micron-scale intermetallic compounds, refined sub-grains, and enhanced mechanical behaviors in the sample. Compared to the sample without treatment, the major contribution to the increasing hardness is from the diffusely distributed intermetallics. This UH technique provides a uniform and homogenous treatment for its controllable static and dynamic loading, which is proved to be a highly efficient approach for improving the micro-hardness of Al alloys.

Declaration of competing interest

The authors declare that they have no known competing financial interests or personal relationships that could have appeared to influence the work reported in this paper.

CRediT authorship contribution statement

Ruixuan Li: Writing - original draft, Visualization, Formal analysis, Writing - review & editing. **Xin Li:** Investigation. **Jiang Ma:** Investigation. **Yong Zhang:** Conceptualization, Methodology, Supervision.

Acknowledgements

Y. Zhang would like to thank the financial support from National Science Foundation of China (Grant Nos. 51471025 and 51671020), and the project of Al–Mg based medium entropy alloys with Dongguan Eontec company. J. Ma would like to thank the financial support from National Science Foundation of China (Grant No. 51871157), and the Science and Technology Innovation Commission Shenzhen (Grants No. JCYJ20170412111216258).

References

[1] G. Liu, G.J. Zhang, F. Jiang, X.D. Ding, Y.J. Sun, J. Sun, E. Ma, Nanostructured high-strength molybdenum alloys with unprecedented tensile ductility, Nat. Mater. 12 (4) (2013) 344–350.
[2] K. Ma, H. Wen, T. Hu, T.D. Topping, D. Isheim, D.N. Seidman, E.J. Lavernia, J. M. Schoenung, Mechanical behavior and strengthening mechanisms in ultrafine grain precipitation-strengthened aluminum alloy, Acta Mater. 62 (2014) 141–155.
[3] W.L. Li, N.R. Tao, K. Lu, Fabrication of a gradient nano-micro-structured surface layer on bulk copper by means of a surface mechanical grinding treatment, Scripta Mater. 59 (5) (2008) 546–549.
[4] H. Chouirfa, H. Bouloussa, V. Migonney, C. Falentin-Daudré, Review of titanium surface modification techniques and coatings for antibacterial applications, Acta Biomater. 83 (2019) 37–54.
[5] A.G. Gutiérrez, P. Sebastian, L.M. Cacho, E.B. Arco, I. Campos, A. Baron, Sci. Surface modification of aluminum alloy 6061 for bipolar plate application: adhesion characteristics and corrosion resistance, Int. J. Electrochem. 13 (2018) 3958–3969.
[6] M. Kheradmandfard, S.F. Kashani-Bozorg, J.S. Lee, C.L. Kim, A.Z. Hanzaki, Y. S. Pyun, S.W. Cho, A. Amanov, D.E. Kim, Significant improvement in cell adhesion and wear resistance of biomedical β-type titanium alloy through ultrasonic nanocrystal surface modification, J. Alloys Compd. 762 (2018) 941–949.
[7] C. Ruirun, Z. Deshuang, G. Jingjie, M. Tengfei, D. Hongsheng, S. Yanqing, F. Hengzhi, A novel method for grain refinement and microstructure modification in TiAl alloy by ultrasonic vibration, Mater. Sci. Eng., A 653 (2016) 23–26.
[8] E.J. Baek, T.Y. Ahn, J.G. Jung, J.M. Lee, Y.R. Cho, K. Euh, Effects of ultrasonic melt treatment and solution treatment on the microstructure and mechanical properties of low-density multicomponent $Al_{70}Mg_{10}Si_{10}Cu_5Zn_5$ alloy, J. Alloys Compd. 696 (2017) 450–459.
[9] F. Wang, D. Eskin, J. Mi, C. Wang, B. Koe, A. King, C. Reinhard, T. Connolley, A synchrotron X-radiography study of the fragmentation and refinement of primary intermetallic particles in an Al-35 Cu alloy induced by ultrasonic melt processing, Acta Mater. 141 (2017) 142–153.
[10] Z. Zhang, Y. Li, J. Peng, P. Guo, J.a. Huang, P. Yang, S. Wang, C. Chen, W. Zhou, Y. Wu, Combining surface mechanical attrition treatment with friction stir processing to optimize the mechanical properties of a magnesium alloy, Mater. Sci. Eng., A 756 (2019) 184–189.

[11] Y. Sun, R. Bailey, A. Moroz, Surface finish and properties enhancement of selective laser melted 316L stainless steel by surface mechanical attrition treatment, Surf. Coating. Technol. 378 (2019) 124993.
[12] X. Zhao, C. Chen, F. Chen, Effect of the precipitated phase of $MgZn_2$ on surface nanocrystallization of Al-Zn-Mg alloy based on high-frequency impacting and rolling, Mater. Lett. 188 (2017) 95–98.
[13] D. Kajánek, B. Hadzima, F. Pastorek, M. Neslušan Jacková, Corrosion performance of AZ31 magnesium alloy treated by ultrasonic impact peening (UIP), Mater. Today: Proceedings 5 (13) (2018) 26687–26692.
[14] K. Zhao, Y. Liu, T. Yao, B. Liu, Y. He, Surface nanocrystallization of Ti–45Al–7Nb–0.3W intermetallics induced by surface mechanical grinding treatment, Mater. Lett. 166 (2016) 59–62.
[15] N. Ao, D. Liu, X. Zhang, C. Liu, J. Yang, D. Liu, Surface nanocrystallization of body-centered cubic beta phase in Ti–6Al–4V alloy subjected to ultrasonic surface rolling process, Surf. Coating. Technol. 361 (2019) 35–41.
[16] A. Amanov, O.V. Penkov, Y.S. Pyun, D.E. Kim, Effects of ultrasonic nanocrystalline surface modification on the tribological properties of AZ91D magnesium alloy, Tribol. Int. 54 (2012) 106–113.
[17] A. Amanov, Y.S. Pyun, J.H. Kim, S. Sasaki, The usability and preliminary effectiveness of ultrasonic nanocrystalline surface modification technique on surface properties of silicon carbide, Appl. Surf. Sci. 311 (2014) 448–460.
[18] J. Ma, X. Liang, X. Wu, Z. Liu, F. Gong, Sub-second thermoplastic forming of bulk metallic glasses by ultrasonic beating, Sci. Rep. 5 (2015) 17844.
[19] F. Luo, F. Sun, K. Li, F. Gong, X. Liang, X. Wu, J. Ma, Ultrasonic assisted micro-shear punching of amorphous alloy, Mater. Res. Lett. 6 (10) (2018) 545–551.
[20] H. Li, Y. Yan, F. Sun, K. Li, F. Luo, J. Ma, Shear punching of amorphous alloys under high-frequency vibrations, Metals 9 (11) (2019) 1158.
[21] J. Ma, C. Yang, X. Liu, Fast surface dynamics enabled cold joining of metallic glasses, Sci. Adv. 5 (11) (2019), eaax7256.
[22] J. Liu, X. Guo, Q. Lin, Z. He, X. An, L. Li, P.K. Liaw, X. Liao, L. Yu, J. Lin, L. Xie, J. Ren, Y. Zhang, Excellent ductility and serration feature of metastable CoCrFeNi high-entropy alloy at extremely low temperatures, Sci. China Mater. 62 (6) (2019) 853–863.
[23] D. Li, Y. Zhang, The ultrahigh charpy impact toughness of forged AlxCoCrFeNi high entropy alloys at room and cryogenic temperatures, Intermetallics 70 (2016) 24–28.
[24] D. Li, C. Li, T. Feng, Y. Zhang, G. Sha, J.J. Lewandowski, P.K. Liaw, Y. Zhang, High-entropy Al0.3CoCrFeNi alloy fibers with high tensile strength and ductility at ambient and cryogenic temperatures, Acta Mater. 123 (2017) 285–294.
[25] Y. Zhang, T.T. Zuo, Z. Tang, M.C. Gao, K.A. Dahmen, P.K. Liaw, Z.P. Lu, Microstructures and properties of high-entropy alloys, Prog. Mater. Sci. 61 (2014) 1–93.
[26] Y. Zhang, High-Entropy Materials: A Brief Introduction, Springer, 2019.
[27] X. Yang, S.Y. Chen, J.D. Cotton, Y. Zhang, Phase stability of low-density, multiprincipal component alloys containing aluminum, magnesium, and lithium, JOM (J. Occup. Med.) 66 (10) (2014) 2009–2020.
[28] Z. Huang, Y. Dai, Z. Li, G. Zhang, C. Chang, J. Ma, Investigation on surface morphology and crystalline phase deformation of $Al_{80}Li_5Mg_5Zn_5Cu_5$ high-entropy alloy by ultra-precision cutting, Mater. Des. 186 (2020) 108367.
[29] R. Sedláček, W. Blum, J. Kratochvíl, S. Forest, Subgrain formation during deformation: physical origin and consequences, Metall. Mater. Trans. 33 (2) (2002) 319–327.
[30] J. Kratochvíl, R. Sedláček, Energetic approach to subgrain formation, Mater. Sci. Eng., A 387–389 (2004) 67–71.
[31] J. Kratochvíl, M. Kružík, R. Sedláček, Statistically based continuum model of misoriented dislocation cell structure formation, Phys. Rev. B 75 (6) (2007), 064104.
[32] J. Kratochvíl, M. Kružík, R. Sedláček, Instability origin of subgrain formation in plastically deformed materials, Int. J. Eng. Sci. 48 (11) (2010) 1401–1412.
[33] J. Zhang, Y.N. Huang, C. Mao, P. Peng, Structural, elastic and electronic properties of θ (Al_2Cu) and S (Al_2CuMg) strengthening precipitates in Al–Cu–Mg series alloys: first-principles calculations, Solid State Commun. 152 (23) (2012) 2100–2104.
[34] Y. Chen, N. Gao, G. Sha, S.P. Ringer, M.J. Starink, Microstructural evolution, strengthening and thermal stability of an ultrafine-grained Al–Cu–Mg alloy, Acta Mater. 109 (2016) 202–212.
[35] Y. Fan, M.M. Makhlouf, Precipitation strengthening in aluminum-zirconium-vanadium alloys, J. Alloys Compd. 725 (2017) 171–180.
[36] K. Ma, T. Hu, H. Yang, T. Topping, A. Yousefiani, E.J. Lavernia, J.M. Schoenung, Coupling of dislocations and precipitates: impact on the mechanical behavior of ultrafine grained Al–Zn–Mg alloys, Acta Mater. 103 (2016) 153–164.
[37] M.A. Hasan, A. Kim, H.J. Lee, Measuring the cell wall mechanical properties of Al-alloy foams using the nanoindentation method, Compos. Struct. 83 (2) (2008) 180–188.